Insights into the impact of self-contained sulfur impurity on the superior photocatalytic activity of UV100

Y. Yan, F. Dappozze, L. Khrouz, F. Lopez-Tenllado, C. Abdou, C. Prevost, A. Marinas, S. Parola, C. Guillard

Insight into the impact of self-contained sulfur impurity on the superior photocatalytic activity of UV100

Yige Yan [a, b], Frederic Dappozze [a], Lhoussain Khrouz [b], Francisco J. López-Tenllado [c], Chadia Abdou [a], Coralie Prevost [a], Alberto Marinas [c], Stephane Parola [b], Chantal Guillard [a *]

[a] *Institut de recherches sur la catalyse et l'environnement de Lyon (IRCELYON), UMR5256, PRETTRE building, 2 avenue Albert Einstein, 69626 Villeurbanne cedex, France*

[b] *Laboratoire de Chimie, ENS de Lyon, 46, allée d'Italie, 69364 Lyon Cedex 07, France*

[c] *Departamento de Química Orgánica, Instituto Químico para la Energía y el Medioambiente (IQUEMA), Universidad de Córdoba, E-14071 Córdoba, Spain*

* Corresponding author:

Dr Chantal Guillard, chantal.guillard@ircelyon.univ-lyon1.fr, +33 [0] 472 445 300

Abstract

Hombikat UV100 is a reference TiO_2 photocatalyst that has been less studied and used than Aeroxide P25. In this work, we evidence that the commercial Hombikat UV100 self-contains non-negligible traces of sulfur as received, and the sulfur can be migrated to the surface of TiO_2 by an easy calcination treatment. This is accompanied by an improved photocatalytic activity in liquid-phase degradation of phenol, paracetamol and chloramphenicol. The reduction in specific surface area induced by heat treatment does not affect the photocatalytic performance. The presence of sulfur delays the transition from anatase to rutile until 700 °C while increasing the crystallinity in anatase phase. A portion of surface sulfate is removable by distilled water as ions along with their associating sodium cations. Such leaching of sulfate and sodium ions did not impact the photocatalytic activity significantly. Although the surface-bound sulfate may act as electron trapping centers or oxygen chemisorb centers, the increased crystallinity in anatase phase by calcining at high temperature thanks to the presence of sulfur may be the origin of the enhanced photocatalytic activity.

Keywords

Photocatalysis, Hombikat UV100 TiO_2, sulfur, emerging contaminant, liquid-phase remediation.

Introduction

Hombikat UV100 is one of the commonly used commercial TiO_2 as a reference in photocatalysis-related studies. Not as frequently used as its homologue Aeroxide TiO_2 P25, the Hombikat UV100 showed some contradictory results in terms of the liquid-phase photocatalytic degradation of pollutants if used directly as received [1-3]. Although the large specific surface area (about 300 m^2/g) [4] and consequent increased surface adsorption capacity [5] are often categorized beneficial to the performance of UV100, other factors such as crystallinity, presence of impurity ions, and the subsequent influence of these ions on the surface/bulk chemistry of the catalyst have never been explicitly studied to the best of our knowledge. The commercial batches of Hombikat UV100 are processed by sulfate approach, where the ilmenite is acidified by concentrated sulfuric acid, followed by hydrolysis, separation and subsequently thermal treatment [6]. The final product is expected to self-contain traces of sulfur element (S). S-doped or S-modified TiO_2 has been purposely synthesized either by *in-situ* means, *i.e.*, by using S-based titanium precursor [7] or by adding S-containing additives with titanium precursors; [2, 8-10] or by post-impregnating synthesized TiO_2 with S-containing solutions. [11, 12] In those studies, the roles of S on photocatalytic activity have been extensively studied and proposed. But surprisingly, the study on a possible influence of the S presence on the surface/bulk chemical and photocatalytic properties of the commercial UV100 photocatalyst is lacking. We have only managed to find a handful number of papers that have reported an increased photocatalytic activity when the UV100 photocatalyst was calcinated at high temperature. [13-15] But no advanced characterizations on the becoming of S after heat treatment, nor a deep investigation on the relationship between the evolution of S, surface/bulk chemistry and the photocatalytic activity in line with the calcination. To this day, the mechanism of the enhanced photocatalytic activity of UV100 after calcination and the related role of S are still elusive.

In the frame of this work, we put in evidence that the commercial Hombikat UV100 indeed self-contains non-negligible traces of sulfur as received, and the sulfur can be migrated to the surface of TiO_2 by a controlled calcination process. This is simultaneously accompanied by the heat-treatment-induced reduction of specific surface area and increased crystallinity in anatase phase. The presence of S delays the thermal transformation from anatase to rutile until 700 °C. The photocatalysts were tested for degradation of three contaminants: Phenol, Paracetamol and Chloramphenicol. Phenol is a major contaminant

whose presence in water can be due to natural occurrence (dead plants and animals decomposition) or through anthropogenic activities (multiple industrial sectors). [16] Its structure is also quite common in different chemicals, such as Paracetamol (analgesic and antipyretic drug) which also contains nitrogen (as an amide group) in its structure. Finally, Cloramphenicol (antibiotic), has been described within the so-called emerging contaminants whose persistence into the aquatic system make them an urgent environmental issue, especially for the development of antimicrobial resistance. [17] Superior photocatalytic degradation performance of these three molecules on UV100 photocatalyst treated at 700 °C as compared to the pristine counterpart was evidenced. Sulfur migrated to the surface was partially found in form of ionic sulfates associating with sodium cations and were subject to be removed by distilled water. The leaching of sulfate and sodium ions had limited impact on the photocatalytic activity.

Results and discussions

Effect of calcination on physico-chemical properties of UV100

A heat treatment of the Hombikat UV100 catalyst resulted in a decreased specific surface area along with an increased mean crystallite size (Figure 1a). The specific surface area of the pristine Hombikat UV100 catalyst is about 307 m^2/g, and gradually decreased to about 18 m^2/g (Table 1) when the UV100 was calcined at 700 °C (UV100-700). The increased mean crystallite size is manifested by a sharpening of diffraction peaks corresponding to anatase phase (*e.g.*, most intense (101) and (004) reflections at 2-Theta values of 25° and 48°, respectively) (Figure 1b). In Raman spectra, typical signals assigned to TiO_2 anatase at 144, 391, 511 and 633 cm^{-1} (corresponding to Eg, B1g, A1g and Eg modes, respectively) are manifested for both UV100 and UV100-700 samples [18] (Figure S1). The calcination resulted in an increase in sharpness of the latter peaks, suggesting an increased crystallinity which is in agreement with XRD results. Raman spectra of pristine UV100 showed a large bump at 3345 cm-1, assigned to the structural OH vibration as well as two unidentified peaks at 219 and 911 cm-1 which disappeared upon calcination at 700 °C. They might be related to the amorphous nature of the pristine UV100.

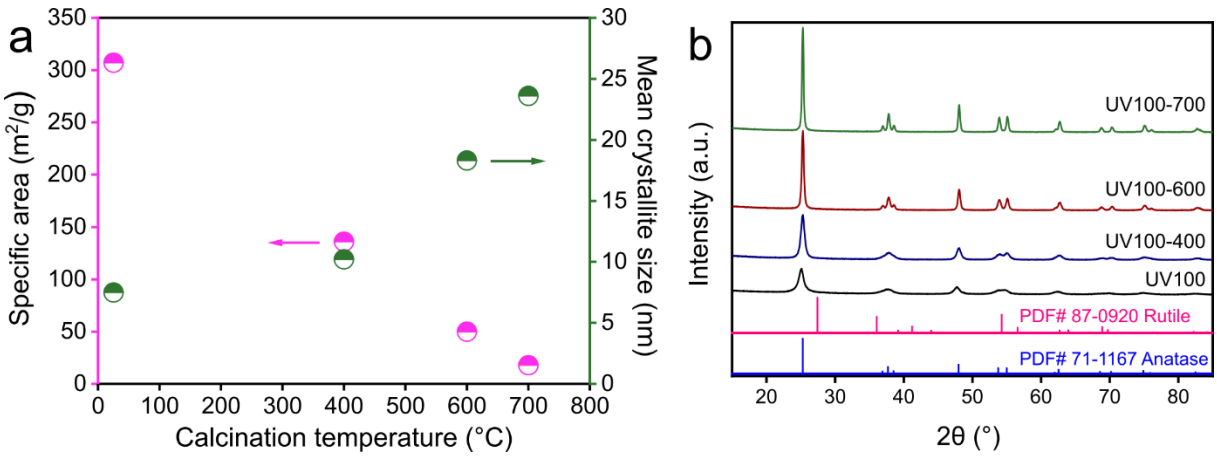

Figure 1. (a) Specific surface area (m^2/g) measured by BET and mean crystallite size (nm) calculated from XRD pattern of pristine UV100 and UV100 calcinated at 400 °C, 600 °C and 700 °C. (b) XRD patterns of UV100 and UV100 calcinated at 400 °C, 600 °C and 700 °C. Rutile and anatase reference patterns are included at the bottom.

Presence of some coordinating elements as impurity in TiO_2 has been reported to inhibit the anatase to rutile transition [19]. In an attempt to quantify the elemental composition of the samples, ICP-OES and XPS analyses revealed non-negligible quantity of sulfur as impurity presence in pristine UV100 and those calcined at different temperatures (Figure 2). The calculated S to Ti atomic percentages from ICP-OES analysis are around 0.2 % regardless of the thermal treatment temperature. However, XPS analyses revealed a significantly higher amount of S to Ti atomic percentage for the pristine UV100 sample (0.79 %), and this value increased with the calcination temperature, up to 2.5 % for UV100-700 (Table 1). Normalized XPS S2p spectra in relative atomic percentage showed an increased intensity of the typical double peaks of S $2p_{3/2}$ and $2p_{1/2}$, corresponding to sulfur element in S^{6+} state, i.e., in sulfate form, with the increasing calcination temperature. The higher sulfur content measured by XPS compared to that measured by ICP-OES for the bare UV100 catalyst suggests that the sulfur elements are preferentially located at the surface of TiO_2 particles rather than being homogeneously distributed in the bulk. Similar observation has been reported for purposely synthesized S-modified TiO_2 [7, 20] but not for the commercially available UV100. The further increased S content by increasing calcination temperature suggested a thermal induced migration of S-based species to the surface of the TiO_2. Similar thermal induced migration of impurity species has been observed for P element in TiO_2 [21, 22] but has been scarcely addressed for S element [20] to the best of our knowledge. The central positions of the $S2p_{3/2}$ and $S2p_{1/2}$ peaks were shifted to higher binding energy from around 167.4eV and 168.8 eV before calcination to 168.3 eV and 169.6 eV after calcination at 700 °C (Figure 2a), suggesting a change in the chemical environment around S elements. Multiple scenarios could

be possible: 1) A transfer from a less oxygen-rich sulfide or oxysulfide form to a more oxygen-rich sulfate form. [23] However, since UV100 catalyst was fabricated in oxidative environment, existence of sulfide or oxysulfide should be counted out. This is also supported by the position of $S2p_{3/2}$ peaks we observed that varied in a range between 167.4 eV and 168.3 eV, which is significantly higher than that of oxysulfide (163.5 eV). 2) Another possibility would be that Titanyl sulfate (or Titanium oxosulfate, $TiOSO_4$) could exist as impurity in pristine UV100 fabricated by sulfate approach, [24] and it changes to sulfate form during calcination. However, according to the literature, the $S2p_{1/2}$ peak position of pure titanyl sulfate is situated at 169.1 eV, [20] similar to that of common sulfate salts (e.g., sodium sulfate), which is situated at 168.9 eV, [25] thus would not result in the shift of S2p spectra we observed. In the end, we think that the thermal-induced shift to higher binding energy for S2p peaks might be attributed to the crystallization or migration of sulfate species initially in dispersed state into clustered state during calcination. Similar suggestion has been made for vanadium in a V-TiO_2 system [26] that the decrease in the degree of the dispersion for the impurity element can result in a shift of binding energy for this element. However, the documentation of this phenomena is lacking for S-TiO_2 system. The presence of S as Ti-O-S bond contribution at lower binding energy was not observed on the Ti2p nor O1s spectra (Figure S2), whatever calcined or not, possibly due to the overall low content of S.

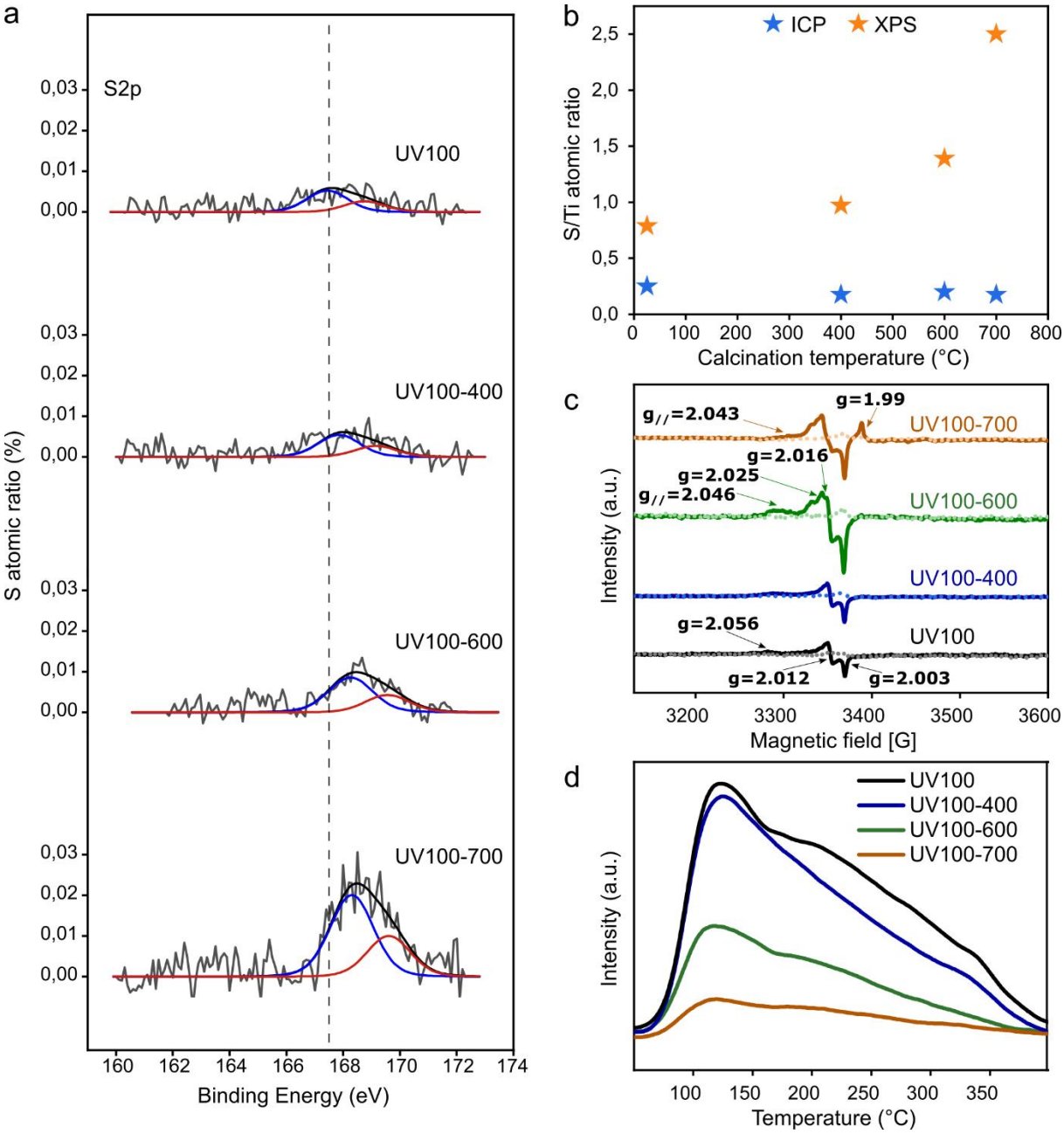

Figure 2. (a) Normalized S2p spectra presented in atomic ratio of sulfur element over all atoms for pristine UV100 and UV100 calcinated at 400 °C, 600 °C and 700 °C. The background has been removed and all spectra have been fitted with $S2p_{3/2}$ and $S2p_{1/2}$ contributions. (b) Atomic ratio of S to Ti deduced from ICP-OES and XPS analyses as a function of calcination temperature on UV100 photocatalyst. (c) EPR spectra of pristine UV100 and UV100 calcinated at 400 °C, 600 °C and 700 °C. Dotted lines are spectra recorded without illumination, solid lines those recorded with a UVA irradiation at 365 nm. (d) pyridine TPD curves up to 400 °C of pristine UV100 and UV100 calcinated at 400 °C, 600 °C and 700 °C.

TGA analysis for pristine UV100 and UV100-700 (Figure S3) revealed a mass loss from 100 °C to 350 °C corresponding to the removal of surface moisture and structure hydroxyl

groups. The pristine UV100 losses much more of its mass in this temperature range compared to its calcinated counterpart, correlating with the much larger specific surface area, thus more surface entities of the former. DSC measurement on the pristine UV100 sample revealed an endothermic peak at 160 °C due to the loss of surface moisture. An exothermic peak around 305 °C is due to the phase transition of TiO_2 from amorphous to anatase [27]. Another mass loss with an onset temperature around 600 °C up to around 900 °C is assigned to the decomposition of metal sulfate salt [28, 29] or metal bisulfate salt. [30] If we presume the common decomposition model (1) for metal sulfate salts at high temperature:

$$l/n\ M(n)_2(SO_4)_n > l/n\ M(n)_2O_n + SO_3 \quad (1)$$

where M is a metal of the oxidation state n. Then the mass loss due to the release of SO_3 gave rise to a calculated S to Ti atomic percentage of 0.13 % for pristine UV100. This value is lower than that measured by ICP-OES (0.25 %, Table 1), which might be a result of an unfinished S migration towards solid surface due to a shorter heating time compared to that adopted to elaborate UV100-700. On the other hand, the calculated S to Ti atomic percentage for the UV100-700 (0.14 %) matches closely with that measured by ICP-OES (0.17 %), suggesting that a calcination at 700 °C for 2h has already completed the sulfur migration on the solid surface, accompanied by partial loss of sulfate/sulfur during the process.

The EPR spectra of UV100 evolve with the calcination temperature (Figure 2c). For pristine UV100, the EPR peaks at $g_1 = 2.056$, $g_2 = 2.012$, and $g_3 = 2.003$ can be attributed to the O_2^{-}° species originating from oxygen adsorbed on the surface of TiO_2. However, the last two peaks can also be explained by $g_{\perp} = 2.012$ and $g_{//} = 2.003$, which are due to the O^{-}° species originating from the trapped photo-generated holes. The first species evolves with the calcination temperature, decreasing to $g_1 = 2.046$ at 600°C and further to $g_1 = 2.043$ at 700°C. This shift of the g factor (g becomes less distorted) is due to changes in the physicochemical environment associated to the thermally induced improved crystallinity. Furthermore, the thermally induced sulfur delocalization from the electron trapping environment sites could also play a role in this shift [31] Two new peaks at g=2.025 and g=2.016 emerge at 600°C, corresponding respectively to two new different species O_2^{-}° and O^{-}° or less axial O^{-}° species. The EPR signals with $g_{\perp} = 1.99$ $g_{//} = 1.96$, assigned to surface electron trapping sites in Ti(III) form (anatase), appear after calcination at 600°C and become more pronounced at 700°C. The sharpness of Ti(III) resonances indicates that Ti(III) centers are located in a more crystalline environment so that the energy levels of Ti(III) centers are high enough to trap photo-

generated electrons. [32] Consequently, it can be concluded that the calcination at 700°C can better inhibit recombination of photogenerated electron/hole pairs.

In situ diffuse reflectance infrared Fourier transform spectroscopy (DRIFTS) in the presence of adsorbed pyridine was used to determine the type of acid sites on the surface for pristine UV100 and UV100-700 (Figure S4). Both samples showed two bands at 1445 cm^{-1} and 1486 cm^{-1} which are attributed to the pyridine ring coordinated to the Lewis acid sites on the surface, while the Brønsted acid sites related bands at 1544 cm^{-1} were not found. [33] Pyridine temperature programmed desorption (TPD) showed a decreased pyridine desorption with the increase in calcination temperatures (Figure 2d). Deconvolution showed four peaks corresponding to pyridine desorption temperature approximately at 105 °C, 154 °C, 241 °C and 358 °C regardless of the calcination temperature (Figure S5). The relative proportions between the weaker acid sites (combining peaks at 105 °C and 154 °C) and the stronger acid sites (combining peaks at 241 °C and 358 °C) are similar for pristine UV100 and all calcinated counterparts (Table S1). All four deconvoluted peaks decreased as a function of increased calcination temperature without any significant alteration to their relative acidity proportions. It appears that neither the calcination nor the migration of sulfate towards surface did alter the acidity type and strength of the acid sites. The total acidity decreased significantly from 0.68 mmol/g to 0.11 mmol/g with increased calcination temperature but note that the specific acidity per surface area increased from 2.2 μmol/m^2 to 6.1 μmol/m^2 (Table 1). A summary of the main characterization results of different UV100-based photocatalysts calcined at different temperatures are shown in Table 1.

Table 1. Summary of main characterization results of different UV100-based photocatalysts calcined at different temperatures.

Sample	Specific surface area (m2/g)	Mean crystallite size (nm)	Acidity		S/Ti atomic percentage (%)		
			Total (mmol/g)	Specific (μmol/m^2)	ICP-OES	XPS	TGA (700-900 °C)
UV100	307	7.5	0.68	2.2	0.25	0.79	0.13
UV100-400	136	10.2	0.56	4.1	0.17	0.97	
UV100-600	50	18.3	0.27	5.4	0.20	1.39	
UV100-700	18	23.6	0.11	6.1	0.17	2.50	0.14

Dissolution of sulfate ions from UV100-based photocatalysts in distilled water

During the photocatalytic degradation in liquid phase, we detected abnormal presence of sulfate and sodium ions in the reaction medium by ionic chromatography. We analyzed the pure distilled water used for photocatalytic tests with and without addition of pollutant

molecules in the same reactor setup and same length of duration, and the sulfate ions were completely absent while sodium ions were at trace level largely inferior to that obtained with the presence of UV100-based samples. This hints that the released sulfate and sodium ions can only be originated from the photocatalysts. Figure S6 shows the evolution of the concentration of sulfate and sodium ions in function of time in an aqueous suspension of 1g/L of UV100 or UV100-700 under moderate stirring. Before addition of TiO_2 photocatalyst, no sulfate ions were detected as expected. Sodium ions were present in trace concentration in blank distilled water. The pristine UV100 released significantly less sulfate ions without reaching the theoretical maximum sulfate concentration (31.2 µmol/L, calculated based on ICP-OES analysis), while UV100-700 released a stable concentration of sulfate that is in the same order as the theoretical maximum bulk sulfate concentration (21.8 µmol/L, calculated based on ICP-OES analysis, Table 2). According to ICP-OES and XPS results, the pristine UV100 does not have all of its S-content at surface that is accessible to water, while for the UV100-700 the S migration towards surface could facilitate the release of sulfate. The concentration of the released sulfate and sodium ions is linearly dependent of the quantity of UV100-700 present in water (Figure 3a). The sodium to sulfate molar ratio for UV100-700 is around 2 in all concentrations, stoichiometrically confirmed that the sulfur existed mostly as Na_2SO_4, explaining their solubility in water.

Vigorous washing of UV100-700 by distilled water (namely UV100-700W), in an *aq.* suspension with a solid concentration of 10g/L for 5 successive times and centrifuged between can result in a significant reduction in solubilized sulfate and sodium content measured (Figure 3b and Table 2). The S to Ti atomic percentage calculated based on mass loss measured by TGA for the UV100-700W sample matches closely to that measured by ICP-OES, which is significantly lower than that in UV100-700 (Table 2). The magnitude of mass loss at around 800 °C is less noticeable after washing (Figure S7). ICP-OES and XPS analyses also confirmed the decrease of S content for UV100-700W (Figure 3c). The S to Ti atomic ratio measured by ICP-OES greatly decreased from 0.17% to 0.03% after washing, while that calculated from XPS data decreased from 2.5% to 1.06% which is still non-negligible. We think that the washing by distilled water is not enough to remove sulfates that absorbed and bound chemically on the surface of the TiO_2. [34, 35] To achieve further elimination of surface sulfate content, we attempted an alkaline washing of UV100-700 in an *aq.* solution of KOH at pH 12 (namely UV100-700WKOH). Potassium hydroxide was chosen instead of sodium hydroxide to avoid incorporation of sodium in TiO_2, insertion of potassium is less probable due to the larger ionic radius. As a result, the alkaline washing indeed was

more effective in removing residue surface sulfate of the photocatalyst. The S to Ti atomic ratio measured by ICP-OES greatly decreased from 0.17% to 0.02% after alkaline washing, while that calculated from XPS data decreased from 2.5% to 0.67% which is near the detection limit for the XPS instrument (Table 2). Figure 3d shows the decreased intensity of S2p peak as different washing methods were applied. It is worth noting that the positions of the S2p peaks were not significantly changed after washing, this suggests that the washing by distilled water and alkaline washing primarily removed soluble sodium sulfate in ions but did not alter the chemical environment around sulfates that still bound to the surface of TiO_2. Pyridine TPD curves and deconvolution profiles of the two samples showed that the two washed samples lost slightly the relative intensity of weakest acid contribution compared to the non-washed counterpart without impacting the total acidity significantly (Figure 3e and Table S1). EPR signal evolution after different washing methods (Figure 3f) will be taken into account to correlate with the photocatalytic results presented later.

Table 2. Influence of washing on some features of UV100-700 photocatalysts.
[a] Na^+ and SO_4^{2-} concentration presented in aqueous suspension of 1g/L TiO_2 measured by ionic chromatography. Na^+ concentrations have been deduced by that presented in blank distilled water.
[b] Na^+ and SO_4^{2-} concentration presented in aqueous suspension of 1g/L TiO_2 if assuming all bulk S (based on ICP-OES measurement) is released.

Sample	Acidity		Ion concentration (µmol/L) 1 g/L TiO_2 *aq.*[a]		Theoretic S concentration (µmol/L) 1 g/L TiO_2 *aq.*[b]	S/Ti atomic percentage (%)		
	Total (mmol/g)	Specific (µmol/m_2)	SO_4^{2-}	Na^+		ICP-OES	XPS	TGA (700-900 °C)
UV100 700	0.11	6.11	21	43	21.8	0.17	2.50	0.14
UV100 700W	0.10	5.56	2.4	11	4.4	0.03	1.06	0.05
UV100 700WKOH	0.12	6.67	0.5	7	2.9	0.02	0.67	-

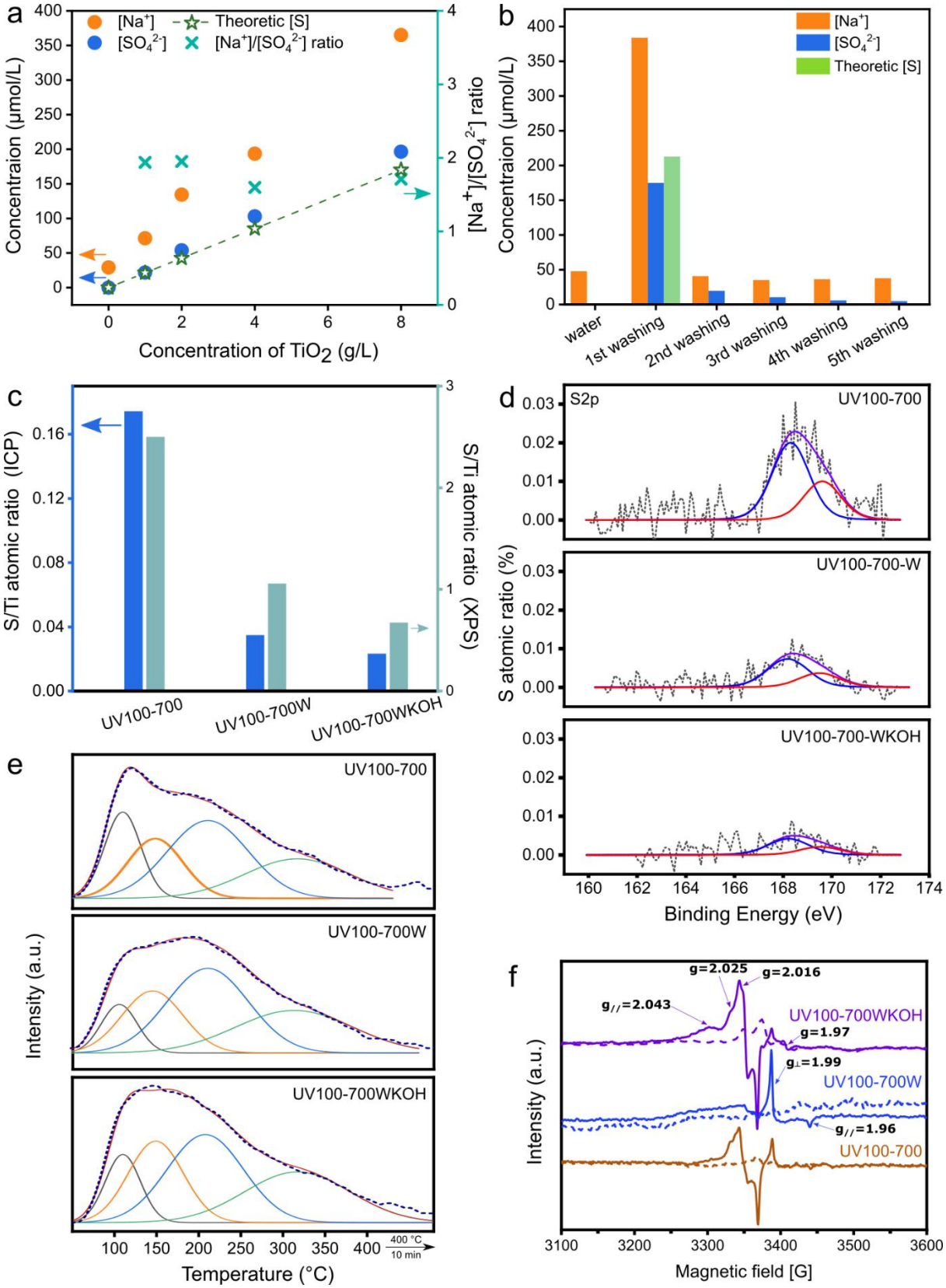

Figure 3. (a) SO_4^{2-}, Na^+ and theoretical S concentration in distilled water as a function of TiO_2 concentration for UV100 calcined at 700 °C (UV100-700). The Na^+ to SO_4^{2-} molar ratio is presented in right Y axis. The theoretical S concentration is calculated based on the ICP-OES analysis result of UV100-700 photocatalyst assuming that all bulk S is released. (b) Effect of washing cycle on the concentration of SO_4^{2-} and Na^+. UV100-700 solid was dispersed in distilled water at a concentration of

10 g/L, the suspension was mixed by 1 min shaking then followed by centrifuge. Concentration of SO_4^{2-} and Na^+ were measured by ionic chromatography in supernatant part, and the solid part was isolated and subsequently washed by same procedure 4 more times. Ions in blank distilled water were measured as reference (labeled as water). (c) S/Ti atomic ratios calculated based on ICP-OES and XPS analyses for UV100-700, UV100 calcinated at 700 °C then washed by distilled water (UV100-700W) and UV100 calcinated at 700 °C then washed by KOH at pH12 (UV100-700WKOH). (d) Normalized S2p spectra presented in atomic ratio of sulfur element over all atoms for UV100-700, UV100-700W and UV100-700WKOH. The background has been removed and all spectra have been fitted with $S2p_{3/2}$ and $S2p_{1/2}$ contributions. (e) Pyridine TPD curves up to 400 °C and their deconvoluted peaks for UV100-700, UV100-700W and UV100-700WKOH. (f) EPR spectra of UV100-700, UV100-700W and UV100-700WKOH. Dotted lines are spectra recorded without illumination, solid lines those recorded with a UVA irradiation at 365 nm.

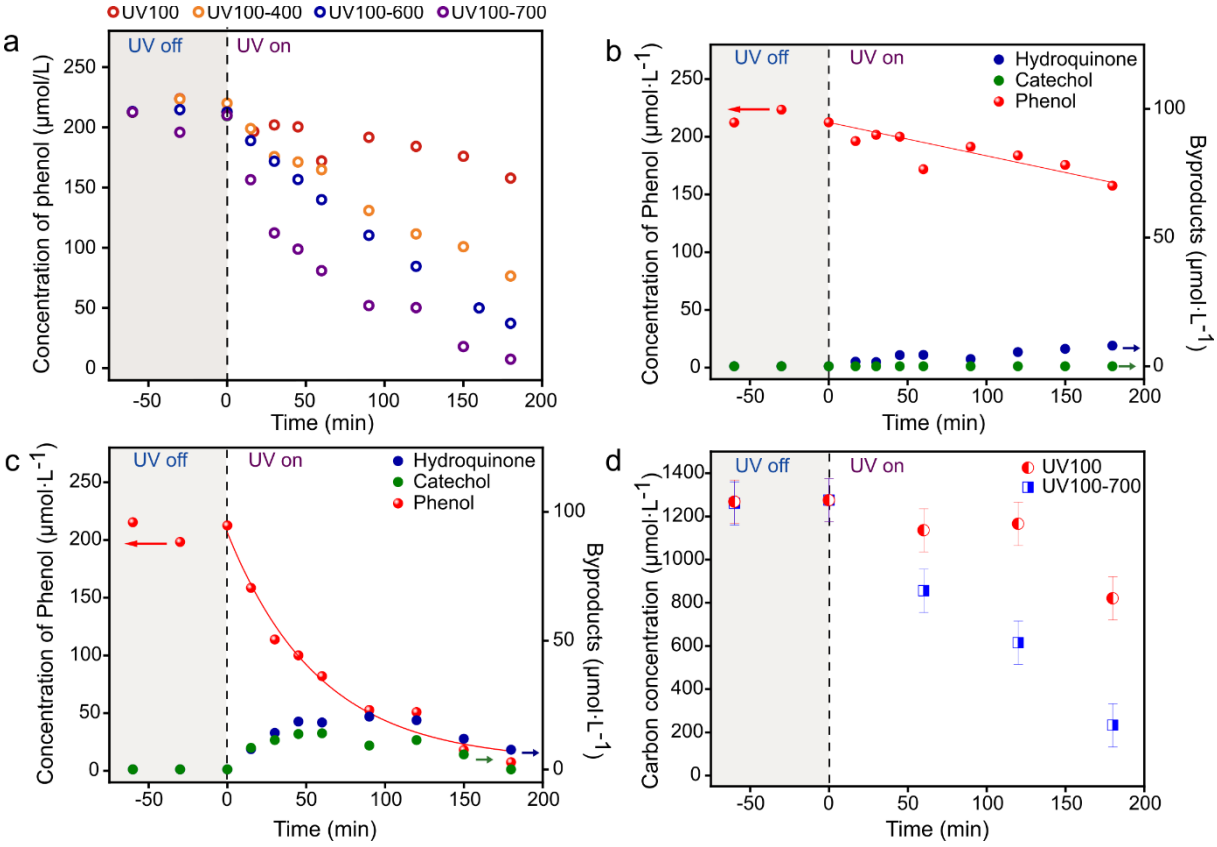

Figure 4. (a) Photocatalytic decay curve of phenol in presence of pristine UV100 and UV100 calcined at 400 °C, 600 °C, 700 °C. (b) Concentration of phenol and generated hydroquinone and catechol concentration as a function of illumination time in presence of pristine UV100. (c) Concentration of phenol and generated hydroquinone and catechol concentration as a function of illumination time in presence of UV100 calcined at 700 °C (UV100-700). The initial concentrations of phenol were targeted to 20 ppm in weight, equivalent to 212.5 µmol/L. All curves have been normalized so that the phenol concentration at Time = -60 min is 212.5 µmol/L. (d) TOC curve of the concentration of carbon left in liquid medium as a function of illumination time for pristine UV100 and UV100-700 photocatalyst.

Photocatalytic performance

Liquid-phase photocatalytic performance in terms of Phenol degradation for pristine UV100 and their calcined homologues are shown in Figure 4. The final conversion rate of Phenol increased significantly from 26% for pristine UV100 to nearly 97% for UV100-700 at the end of 3 hours of illumination time. Generation of Hydroquinone and Catechol as intermediate degradation products of Phenol was followed. While these 2 products were still in ascendant phase for the pristine UV100 at the end of 3 hours of illumination time, they already entered a descendant phase for UV100-700 at same reaction time. In line with the plateaued TOC curve (Figure 4d), the degradation of Phenol on pristine UV100 mainly consisted in hydroxylation of Phenol at early stage of reaction. Cleavage of aromatic C=C and oxidation of hydrocarbon species into CO_2 did not occur at a significant rate. On the contrary, for the UV100-700, degradation of Phenol was accompanied by formation and degradation of by-products simultaneously, which is manifested by the linear decrease of TOC curve during the whole duration of the reaction. No correlation between specific surface area (i.e., number of active sites) and photocatalytic performance was observed for all photocatalysts. It seems that the adsorption capacity is not the limiting factor, but the intrinsic photocatalytic activity is determinant for the faster degradation of Phenol.

Photocatalytic degradation tests results of Paracetamol and Chloramphenicol in presence of pristine UV100 and UV100-700 are depicted in Figure 5. Paracetamol and Chloramphenicol undergo successive long photocatalytic degradation steps starting from aromatic addition/substitution reaction, breakdown of aromatic compound to smaller carboxylic chains to finally mineralization. Identifying and quantifying a full list of organic intermediate molecules for the degradation of these two pollutants are not the goal of this paper, readers can refer the works done by Yang *et al.* [36] and Chatzitakis *et al.* [37] for this purpose. We are interested in the original molecule decay rate and the final mineralization yield. The mineralization products are CO_2 for carbon-based compounds as well as NH_4^+/NO_3^- and Cl^- if the starting molecule contains nitrogen or chlorine atoms.

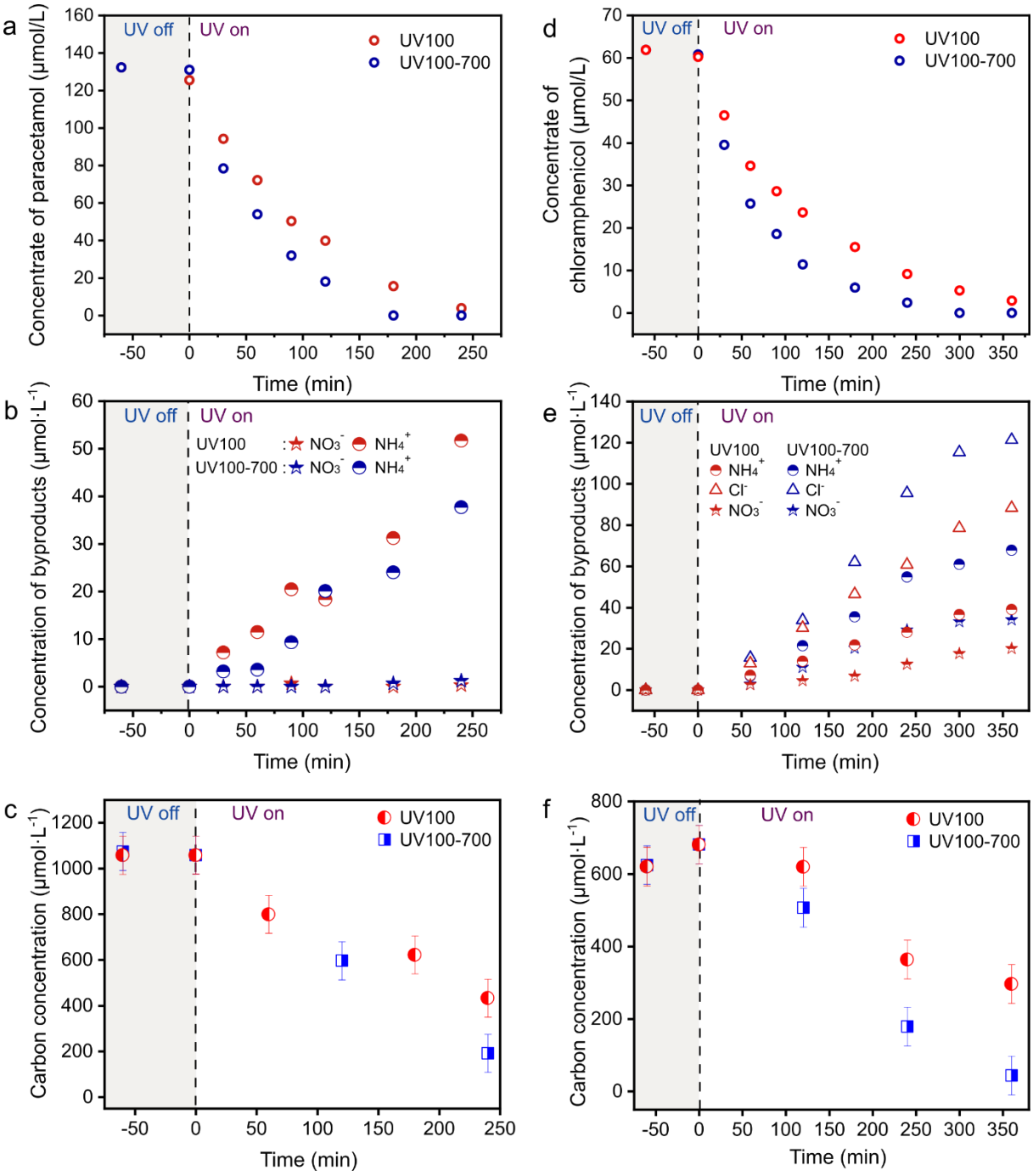

Figure 5. (a) Photocatalytic decay curve of paracetamol in the presence of pristine UV100 and UV100 calcined at 700 °C (UV100-700). The initial concentrations of paracetamol were set at 20 ppm in weight, equivalent to 132.3 µmol/L. All curves have been normalized so that the paracetamol concentration at Time = -60 min is 132.3 µmol/L. (b) Concentration of nitrate and ammonium ions from degradation of paracetamol as a function of illumination time in presence of pristine UV100 and UV100-700. (c) TOC curve of the concentration of carbon remaining in the liquid medium as a function of illumination time for the degradation of paracetamol in presence of pristine UV100 and UV100-700 photocatalyst. (d) Photocatalytic decay curve of chloramphenicol in the presence of pristine UV100 and UV100-700. The initial concentrations of chloramphenicol were set at 20 ppm in weight, equivalent to 61.9 µmol/L. All curves have been normalized so that the chloramphenicol concentration at Time = -60 min is 61.9 µmol/L. (b) Concentration of nitrate, ammonium and chloride ions as a function of illumination time from the degradation of chloramphenicol in the presence of pristine UV100 and UV100-700. (c) TOC curve of the concentration of carbon remaining in the liquid

medium as a function of illumination time from the degradation of chloramphenicol in presence of pristine UV100 and UV100-700 photocatalyst.

For Paracetamol, UV100-700 presented higher Paracetamol decay rate and TOC decay curve than pristine UV100. The amplitude of improvement for Paracetamol degradation as a result of a calcination at 700 °C is less pronounced than that for Phenol degradation. Ammonium is the major mineralization product of nitrogen for both photocatalysts, and the nitrogen mineralization rates are around 41% for pristine UV100 and 29% for UV100-700 at a reaction time of 240 min. However, the TOC analyses showed significantly better carbon mineralization rate for UV100-700 (82%) than that of pristine UV100 (59%) at the same reaction time. It seems that the calcination treatment did improve the degradation rate and the carbon mineralization rate of Paracetamol significantly, however the nitrogen mineralization process is not improved and remains to be the most difficult step to achieve.

For Chloramphenicol, after 350 min irradiation, the carbon and nitrogen mineralization values observed for UV100-700 (94% and 82% respectively) are greater than those of the pristine UV100 (56% and 50% respectively). It is worth noting that the nitrate formation is more pronounced here than for paracetamol degradation, due to the presence of nitro group in Chloramphenicol that can be oxidized into nitrate more easily than the other half that existed as secondary amine (Figure S8). Finally, chlorine mineralization rate almost reached a completion (98%) for UV100 700 as opposed to 75% for pristine UV100 at the end of 360 min. The near total chlorine mineralization is in correlation with that the chloride formation curve entered in a plateau phase at the end.

Table 2. Decay rate constant, fitted by a first order exponential decay model, for the degradation of different molecules and in presence of different UV100-based photocatalysts. Effect of calcination on UV100 and the effect of washing on UV100-700 can be seen in phenol degradation rate.
* Impractical for a first order exponential decay fit.

Sample	Phenol decay rate constant (s^{-1})	Paracetamol decay rate constant (s^{-1})	Chloramphenicol decay rate constant (s^{-1})
UV100	Near zero*	0.00793	0.00812
UV100-400	0.00426	-	-
UV100-600	0.00474	-	-
UV100-700	0.00950	0.01439	0.01360
UV100-700W	0.00813	-	-
UV100-700WKOH	0.00467	-	-

Impact of washing on photocatalytic activity

The removal of sulfates by distilled water on UV100-700 had only marginal impact on the photocatalytic performance on the degradation of Phenol. Figure 6a shows that the exponential shape of the Phenol degradation curves slightly changed from UV100-700 to UV100-700WKOH, but still remain much more efficient compared to that of the pristine UV100. The average rate constants of the first order decay of Phenol, obtained by averaging the rate constants of three repetitive tests, decreased from $9.50x10^{-3}$ s^{-1} for UV100-700 to $8.13x10^{-3}$ s^{-1} for UV100-700W and finally to $4.67x10^{-3}$ s^{-1} for UV100-700WKOH (Table 2). Repetitive test of Phenol degradation in the presence of all three photocatalysts indeed showed good reproducibility (Figure S9), thus validating these differences. TOC curves also follow a slight decreased mineralization rate in an order of UV100-700 > UV100-700W > UV100-700WKOH (Figure 6b). The slight decrease of weak acidic site amount observed after washing (Figure 3e and Table S1) could impact the absorption of Phenol or its aromatic by-products (e.g., Hydroquinone, Catechol), thus influencing the overall photocatalytic mineralization rate. However, we did not find literature support regarding this assumption. Furthermore, no significant change of the intensity for weakest Lewis acid sites (Peak 1 in Table S1) has been noticed between UV100-700W and UV100-700WKOH, yet their reaction rate constants differed. The released sulfate concentrations in presence of all three photocatalysts were stable during the whole test (Figure S10), suggesting that the UVA irradiation or the photocatalytic reaction did not impact the release of sulfate ions. Reciprocally, to see if the presence of the sulfate ions impacts the photocatalytic activity, we added adequate amount of sodium sulfate (i.e. similar amount as released by UV100-700) in the reaction medium for UV100-700W and UV100-700WKOH phenol degradation tests (labeled as "UV100-700WS" and "UV100-700WKOHS" respectively, Figure S11). No significant difference was noticed between UV100-700W and UV100-700WS, nor between UV100-700WKOH and UV100-700WKOHS. As expected, the free sulfate ions in the reaction medium did not impact the photocatalytic degradation of phenol. Contrary, the washing resulted in noticeable impacts on the surface chemistry of the photocatalysts. Although the surface change is not evident by SEM observations (Figure S12), The EPR spectra revealed more details. UV100-700W showed a significantly more intense EPR resonance at g=1.99 (related to surface electron trapping sites in Ti(III) anatase) compared to its non-washed counterpart (Figure 3f). This indicated that the majority of photo-generated electrons are found trapped on the surface, reducing surface Ti centers to Ti(III), after washing by distilled water. Consequently, we hypothesize that the surface sulfur content

might play a role as a chemisorption center for oxygen molecules or as an electron withdrawer to transfer photo-generated electrons to surface adsorbed oxygen. [34] In either case, the reduction in surface sulfur content by washing might result in lack of means for the photo-generated electrons to efficiently transfer to surface adsorbed electron accepters in air, thus they mostly end up being trapped in Ti(III) sites. However, the lack of sulfur by itself did not impact significantly the photocatalytic activity. It appears that the presence of sulfur is not correlated to the total amount of holes and electrons photo-generated, and the photo-generated species could have been efficiently used in liquid-phase redox reaction of pollutants. The UV100-700WKOH on the other hand differs in a more distinguishable manner in EPR spectrum by showing two new species that are originated from shifted signals corresponding to the trapping of surface electrons at g = 2.043 ($O_2^{-\circ}$) and g = 1.97 (Ti(III)), respectively. The shift in these values can be explained by the change in the physical environment of the trapped electrons due to the decrease in crystallinity. Indeed, XRD pattern of the UV100-700WKOH sample showed broader peak width than that of the UV100-700 and UV100-700W counterparts (Figure S13). It suggests that the washing by KOH solution impacted the crystal integrity of TiO_2, perhaps by surface corrosion, so that the surface amorphous region has no longer a large enough band-gap to retain photo-generated holes and electrons separated; thus, explaining the lowered photocatalytic activity of this photocatalyst.

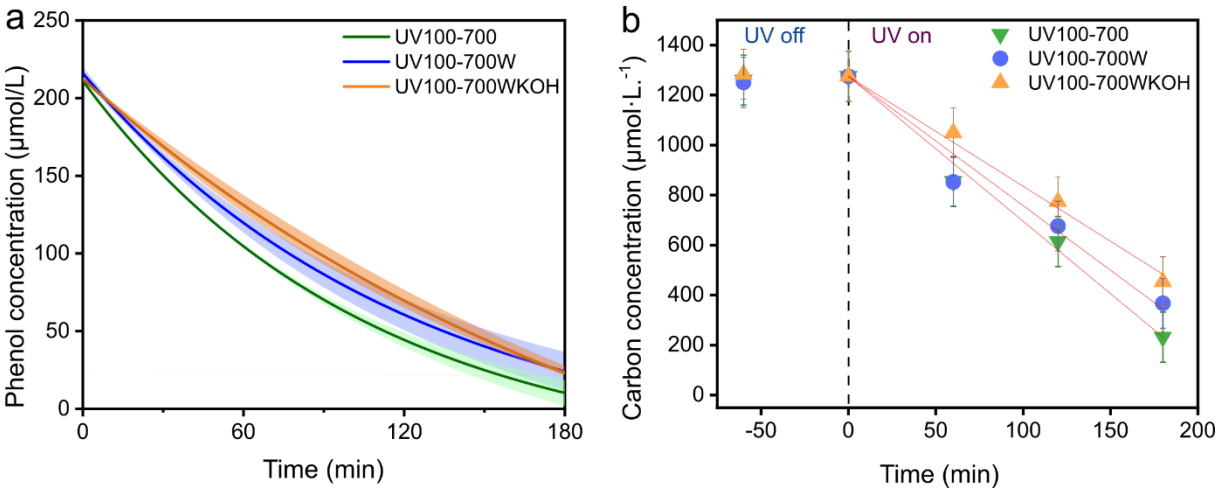

Figure 6. (a) First order fit of the photocatalytic decay curves of phenol in presence of UV100-700, UV100-700W and UV100-700WKOH. Three tests have been repeated and the mean phenol decay curves are fitted by first order decay model and are presented as solid lines, along with colored error bands. The individual curves of repeat tests are shown in SI. (b) TOC curves of the photocatalytic degradation of phenol in presence of UV100-700, UV100-700W and UV100-700WKOH.

The quantity of the sulfates actually bound to the surface of UV100-700 during the reaction, after the dissolution of most of them by distilled water, is extremely low in our case and is difficult to quantify. By itself, this low quantity of surface sulfate bound to UV100-700 cannot justify the magnitude of photocatalytic activity improvement compared to the pristine UV100. We think that the main origin of this improvement is the retard in anatase to rutile transition thanks to the presence of sulfur as impurity, which resulted in highly crystalline anatase phase after calcination at a high temperature. Anatase phase in higher crystallinity is beneficial at generating electron-hole pairs and avoiding charge recombination, which correlates with the EPR results of the UV100-700 photocatalyst showing both distinguished trapping hole signals and trapping electron signal compared to the pristine UV100. Thanks to the self-presence of sulfur, the calcination of pristine UV100 at 700 °C is a reasonable compromise temperature to increase the crystallinity while retaining anatase phase.

Conclusion

In the frame of this work, we evidenced that the commercial Hombikat UV100 self-contains non-negligible traces of sulfur as received. Furthermore, an easy calcination treatment can greatly enhance the photocatalytic activity in liquid-phase degradation of phenol, paracetamol and chloramphenicol. This enhancement is accompanied by an increased crystallinity of the anatase phase and a migration of sulfur to the surface of TiO_2 during calcination. The presence of sulfur retards the anatase-to-rutile transition, resulting in a highly crystalline anatase phase after calcination at high temperature, which is the primary reason for the improved photocatalytic activity. Sulfur migrates to the surface of TiO_2 and forms sulfate upon thermal treatment. Despite a portion of which was associated with sodium and was removable by distilled water, an extremely low portion of sulfate remained bound to the surface of TiO_2 and might act as electron trapping centers or oxygen chemisorb centers. The heat-treatment-induced reduction of specific surface area was not impactful on the photocatalytic performance. The leaching of sulfate and sodium ions in water also had limited impact on the photocatalytic activity. We believe that our findings offer novel and enduring insights into the photocatalytic properties of the understudied Hombikat UV100 TiO_2 reference.

Experimental

Sample preparation

Commercial Hombikat UV100 was purchased from Sachtleben Chemie GmbH, and was used as received. The pristine UV100 sample was named as "UV100" and was served as our reference to be compared with. Calcinations were carried out on UV100 to yield "UV100-X", where X is the calcination temperature in Celsius. Calcinations were performed under air with a heating rate of 5 °C·min^{-1} then kept at the desired temperature for 2h. After cooled to room temperature, the photocatalyst in powder form was used in photocatalytic test as obtained.

To study the effect of washing on photocatalytic performance, the most effective one "UV100-700" was washed to reduce sulfur content. In detail, 0.4 g of UV100-700 powder was suspended in 40 ml distilled water hand shaked for 1 min. Then the solid was isolated by centrifugation at 4000 RPM for 20 min and consecutively washed 4 more times by repeating the same procedure. The final product was isolated and dried in air at room temperature and labeled as UV100-700W. Alkaline wash of UV100-700 was performed by a similar protocol, in which the first washing was carried on in a solution of KOH at pH=12. The solid was then isolated by centrifugation and consecutively washed 4 more times by distilled water so that the supernatant reached a neutral pH. The final product was isolated and dried in air at room temperature and labeled as UV100-700WKOH.

Characterization

Phase identification of dried powders was carried out by X-ray diffraction (XRD) with an Empyrean X-ray diffractometer (Malvern Panalytical) using CuK$\alpha_{1,2}$ radiation in the Bragg-Brentano configuration.

Electron paramagnetic resonance (EPR) assays were all carried out with and without an irradiation of 365nm (Thorlab LED) at room temperature and 100K using a Bruker E500 spectrometer operating at X-band (9.4 GHz), rectangular cavity (ST520), with 100 KHz modulation frequency. The instrument settings were as follows: microwave power: 69mW, modulation amplitude: 2 G.

Scanning Electron Microscopy (SEM) observations were performed using a JEOL IT800 scanning electron microscope equipped with In-Lens Schottky Plus Field Emission Election Gun (FEG).

ICP-OES analysis was adopted to quantify the S/Ti atomic ratio of different photocatalysts. Samples were dissolved in hot HNO_3/HF medium prior to analyses by an Agilent 5800 ICP-OES instrument.

X-ray photoelectron spectra (XPS) were conducted at the Central Service for Research Support (SCAI) of the University of Córdoba using a Phoibos 150 MCD (Specs, Germany) instrument with an AlKα (hν = 1486.6 eV) X-ray source and operating at 400 W. Samples were compressed into pellets and subsequently outgassed to a pressure below $6x10^{-9}$ mbar at room temperature. High-resolution spectra were recorded for Ti2p, O1s, S2p and C1s and the signal of C1s was used as the reference (284.8 eV).

Acidity studies were carried out using pyridine as the probe molecule. Studies on the type of acid sites (Brönsted or Lewis) were performed using Diffuse Reflectance Infrared Fourier Transform Spectroscopy (DRIFTS) on a Fourier-transform infrared spectroscopy (FTIR) instrument (Perkin Elmer Frontier) equipped with an environmental chamber (Harrick HVC-DRM). A resolution of 4 cm^{-1} was used with 125 scans averaged to obtain a spectrum from 4000 to 400 cm^{-1}. Before each test the solids were heated at 150°C and then pyridine adsorption was conducted at 100ºC for 45 min to achieve the saturation of the catalyst surface. The physically adsorbed pyridine was then removed from the surface with an Ar flow (50 mL min^{-1}). Finally, the infrared radiation (IR) spectra were recorded at 150 °C taking as the reference the solid submitted to the same treatment but without pyridine.

Quantitative determination of surface acidity was carried out by pyridine Temperature Programmed Desorption (TPD) using a thermal conductivity detector (TCD). The sample (50 mg) was introduced into a reactor and submitted to a helium flow of 10 mL/min. Initially, the solid was heated up to 400°C at a rate of 10 °C/min and maintained at this temperature for one hour to clean the surface. Subsequently, the temperature was lowered to 50°C, and the solid surface was saturated with pyridine for 30 minutes, being pyridine introduced by bubbling the helium stream through liquid pyridine at room temperature. Following saturation, any excess of physisorbed pyridine was eliminated by passing a flow of helium at 50°C for 1 hour. Desorption was then initiated by ramping up the temperature to 400°C at a rate of 10 °C/min, with the final temperature held for 15 minutes.

Raman spectra were recorded by a LabRam HR Evolution spectrometer using a 532 nm Laser as source.

Thermogravimetry (TGA) measurement was performed on a Setaram LABSYS1600 analyzer coupled with Differential Scanning Calorimetry (DSC) heat flow measurement.

Photocatalytic tests

Photocatalytic degradation tests were conducted by using a 100 ml Pyrex photo-reactor in air atmosphere. Phenol (99%, Aldrich-Sigma), Paracetamol (99%, Aldrich-Sigma) or Chloramphenicol (99%, Aldrich-Sigma) were used as pollutants. For all the experiments, the concentration of the photocatalyst was set to 1 $g \cdot L^{-1}$. In detail, 100 mg of catalyst were added to 100 mL of a solution of the pollutant (20 ppm) with top motorized stirring for 60 min in the dark to reach equilibrium. A pre-heated UV-A PL-L 18W (Philips) was positioned under the reactor. The irradiation at 365 nm measured on the inner bottom side of the reactor was 4.8 mW/cm^2. 0.8 mL of the solution was sampled and filtrated on an MILLEX HVLP 0.45 µm hydrophilic filter (Millipore, Burlington, MA, USA) for the HPLC analyses.

HPLC analyses for phenol and paracetamol were performed using a Shimadzu system (Shimadzu, Japan) equipped with a photodiode array detector and a 150 mm × 4.6 mm x 2,7µm-Ascentis Express 90 A° AQ-C18 column (Supelco Merck). The mobile phase was a 95 %v / 5% v acidified Water (with 0.1%w/w HCOOH) / Methanol mixed solution.

HPLC analyses of chloramphenicol were performed using VARIAN ProStar system with a photodiode array detector and a 250 mm × 4.6 mm x 5µm-Nucleodur C18 HTec reverse-phase column (Macherey Nagel). The mobile phase composition was methanol and acidified water (with 0.1% w/w of formic acid to pH = 3) at a volume ratio of 40:60.

In all cases the flow rate was set at 1.0 mL.min−1. All of the HPLC analysis were performed at 40 °C.

Reaction rate constant for the first order decay kinetics was calculated by the formula (3):

$$\frac{[A]_{1/2}}{[A]_0} = \frac{1}{2} = e^{-kt_{1/2}} \quad (3)$$

Where $[A]_0$ is the initial concentration of the molecule A after absorption period in the dark, $[A]_{1/2}$ is the concentration of $[A]_0$ decreased by half, $t_{1/2}$ is the timescale on which the initial concentration $[A]_0$ is decreased by half. K is the reaction rate constant presented in s^{-1}.

Ionic chromatography was used to trace the concentration of NH_4^+/NO_3^- and Cl^- if the original molecule contains nitrogen or chlorine atoms. The instrument was a Metrohm 881 Compact IC pro. Two column, thermostated at 30 °C, were used : Metrosep C4 150/4.0 for cations and Metrosep A supp5 150/4.0 for anions. The mobile phases were mixtures of both 1.7mM nitric acid and 0.7mM of dipicolinic acid for cations, and of 3.2mM sodium carbonate and 1mM sodium hydrogenocarbonate for anions. Both flow rates were 1ml/min. Conductivity detector suppression was made by a 0.1M Phosphoric acid solution.

The Total Organic Carbon (TOC) of phenol was quantified during photocatalytic tests at different times using a Shimadzu TOC-VSCH model equipped with an autosampler. The detection limit of the TOC analyzer is 0.5 $mg \cdot L^{-1}$ and the quantification limit is 1 $mg \cdot L^{-1}$.

Acknowledgements

This work is carried on in the frame of the collaborative international consortium GreenWaterTech financed under the ERA-NET AquaticPollutants Joint Transnational Call (GA no. 869178). The ERA-NET is an integral part of the activities developed by the Water, Oceans and AMR Joint Programming Initiatives. Anne Bonhomme of IRCELYON is thanked for Raman analysis. Pascale Mascunan and Nicolas Bonnet of IRCELYON are acknowledged for ICP-OES and BET measurements. Thibaut Cornier of IRCELYON is thanked for the TGA-DSC analyses. FJLT and AM are grateful to MICINN (PID2022-142275OB-I00/ AEI/10.13039/501100011033 and FEDER funds).

Bibliography

[1] C.A. Emilio, M.I. Litter, M. Kunst, M. Bouchard, C. Colbeau-Justin, Phenol Photodegradation on Platinized-TiO2 Photocatalysts Related to Charge-Carrier Dynamics, Langmuir, (2006) 3606-3613.
[2] H. Li, G. Li, J. Zhu, Y. Wan, Preparation of an active SO42−/TiO2 photocatalyst for phenol degradation under supercritical conditions, J. Mol. Catal. A: Chem., 226 (2005) 93-100.
[3] Y. Ji, L. Zhou, C. Ferronato, X. Yang, A. Salvador, C. Zeng, J.-M. Chovelon, Photocatalytic degradation of atenolol in aqueous titanium dioxide suspensions: Kinetics, intermediates and degradation pathways, Journal of Photochemistry and Photobiology A: Chemistry, 254 (2013) 35-44.
[4] A. Alonso Tellez, R. Masson, D. Robert, N. Keller, V. Keller, Comparison of Hombikat UV100 and P25 TiO_2 performance in gas-phase photocatalytic oxidation reactions, Journal of Photochemistry and Photobiology A: Chemistry, 250 (2012) 58-65.
[5] T.E. Doll, F.H. Frimmel, Removal of selected persistent organic pollutants by heterogeneous photocatalysis in water, Catal. Today, 101 (2005) 195-202.
[6] P.S. Croce, A. Mousavi, A sustainable sulfate process to produce TiO2 pigments, Environmental Chemistry Letters, 11 (2013) 325-328.
[7] X.H. Lin, S.F.Y. Li, Impact of the spatial distribution of sulfate species on the activities of SO42−/TiO2 photocatalysts for the degradation of organic pollutants in reverse osmosis concentrate, Applied Catalysis B: Environmental, 170-171 (2015) 263-272.
[8] C. Zhan, F. Chen, H. Dai, J. Yang, M. Zhong, Photocatalytic activity of sulfated Mo-doped TiO2@fumed SiO2 composite: A mesoporous structure for methyl orange degradation, Chem. Eng. J., 225 (2013) 695-703.
[9] E. Zhang, Y. Pan, T. Lu, Y.a. Zhu, W. Dai, Novel synthesis of S-doped anatase TiO2 via hydrothermal reaction of Cu–Ti amorphous alloy, Appl. Phys. A, 126 (2020).
[10] J.-H. Xu, J. Li, W.-L. Dai, Y. Cao, H. Li, K. Fan, Simple fabrication of twist-like helix N,S-codoped titania photocatalyst with visible-light response, Applied Catalysis B: Environmental, 79 (2008) 72-80.
[11] B.M. Reddy, P.M. Sreekanth, Y. Yamada, Q. Xu, T. Kobayashi, Surface characterization of sulfate, molybdate, and tungstate promoted TiO2-ZrO2 solid acid catalysts by XPS and other techniques, Applied Catalysis A: General, 228 (2002) 269-278.
[12] G. Colón, M.C. Hidalgo, J.A. Navío, A. Kubacka, M. Fernández-García, Influence of sulfur on the structural, surface properties and photocatalytic activity of sulfated TiO2, Applied Catalysis B: Environmental, 90 (2009) 633-641.
[13] J. Kirchnerova, M.L. Herrera Cohen, C. Guy, D. Klvana, Photocatalytic oxidation of n-butanol under fluorescent visible light lamp over commercial TiO2 (Hombicat UV100 and Degussa P25), Applied Catalysis A: General, 282 (2005) 321-332.
[14] W. Ruu Siah, H. O. Lintang, M. Shamsuddin, L. Yuliati, Effect of calcination temperatures on the photocatalytic activities of commercial titania nanoparticles under solar simulator irradiation, Malaysian Journal of Fundamental and Applied Sciences, 11 (2015).
[15] V.A. Lebedev, D.A. Kozlov, I.V. Kolesnik, A.S. Poluboyarinov, A.E. Becerikli, W. Grünert, A.V. Garshev, The amorphous phase in titania and its influence on photocatalytic properties, Applied Catalysis B: Environmental, 195 (2016) 39-47.
[16] K.A. Mohamad Said, A.F. Ismail, Z. Abdul Karim, M.S. Abdullah, A. Hafeez, A review of technologies for the phenolic compounds recovery and phenol removal from wastewater, Process Safety and Environmental Protection, 151 (2021) 257-289.
[17] G. Lofrano, G. Libralato, R. Adinolfi, A. Siciliano, P. Iannece, M. Guida, M. Giugni, A. Volpi Ghirardini, M. Carotenuto, Photocatalytic degradation of the antibiotic chloramphenicol and effluent toxicity effects, Ecotoxicology and Environmental Safety, 123 (2016) 65-71.
[18] L. Chu, Z. Qin, J. Yang, X. Li, Anatase TiO2 Nanoparticles with Exposed 001 Facets for Efficient Dye-Sensitized Solar Cells, Scientific reports, 5 (2015) 12143.

[19] D.A.H. Hanaor, C.C. Sorrell, Review of the anatase to rutile phase transformation, Journal of Materials Science, 46 (2011) 855-874.
[20] F.G. Svensson, L. Österlund, One‐Step Synthesis of Sulfate‐Modified Titania Nanoparticles with Surface Acidic and Sustained Photocatalytic Properties via Solid‐State Thermolysis of Titanyl Sulfate, ChemCatChem, 14 (2022).
[21] K. Elghniji, M.E. Saad, M. Araissi, E. Elaloui, Y. Moussaoui, Chemical modification of TiO_2 by $H_2PO_4^-$/HPO_4^{2-} anions using the sol-gel route with controlled precipitation and hydrolysis: enhancing thermal stability, Materials Science-Poland, 32 (2014) 617-625.
[22] Y. Yan, V. Keller, N. Keller, On the role of $BmimPF_6$ and P/F- containing additives in the sol-gel synthesis of TiO_2 photocatalysts with enhanced activity in the gas phase degradation of methyl ethyl ketone, Applied Catalysis B: Environmental, 234 (2018) 56-69.
[23] D. Gonbeau, C. Guimon, G. Pfister-Guillouzo, A. Levasseur, G. Meunier, R. Dormoy, XPS study of thin films of titanium oxysulfides, Surf. Sci., 254 (1991) 81-89.
[24] F. Zeng, D. Luo, Z. Zhang, B. Liang, X. Yuan, L. Fu, Study on the behavior of sulfur in hydrolysis process of titanyl sulfate solution, J. Alloys Compd., 670 (2016) 249-257.
[25] M. Wahlqvist, A. Shchukarev, XPS spectra and electronic structure of Group IA sulfates, J. Electron. Spectrosc. Relat. Phenom., 156-158 (2007) 310-314.
[26] M. Kobayashi, M. Hagi, V2O5-WO3/TiO2-SiO2-SO42− catalysts: Influence of active components and supports on activities in the selective catalytic reduction of NO by NH3 and in the oxidation of SO2, Applied Catalysis B: Environmental, 63 (2006) 104-113.
[27] J.R. Sohn, D.C. Shin, Environmentally friendly solid acid catalyst prepared by modifying TiO2 with cerium sulfate for the removal of volatile organic chemicals, Applied Catalysis B: Environmental, 77 (2008) 386-394.
[28] J. Mu, D.D. Perlmutter, Thermal decomposition of inorganic sulfates and their hydrates, Industrial & Engineering Chemistry Process Design and Development, 20 (1981) 640-646.
[29] H. Tagawa, Thermal decomposition temperatures of metal sulfates, Thermochim. Acta, 80 (1984) 23-33.
[30] K.J. De Vries, P.J. Gellings, The thermal decomposition of potassium and sodium-pyrosulfate, J. Inorg. Nucl. Chem., 31 (1969) 1307-1313.
[31] C.P. Kumar, N.O. Gopal, T.C. Wang, M.-S. Wong, S.C. Ke, EPR Investigation of TiO2 Nanoparticles with Temperature-Dependent Properties, The Journal of Physical Chemistry B, 110 (2006) 5223-5229.
[32] R. Scotti, I.R. Bellobono, C. Canevali, C. Cannas, M. Catti, M. D'Arienzo, A. Musinu, S. Polizzi, M. Sommariva, A. Testino, F. Morazzoni, Sol−Gel Pure and Mixed-Phase Titanium Dioxide for Photocatalytic Purposes: Relations between Phase Composition, Catalytic Activity, and Charge-Trapped Sites, Chem. Mater., 20 (2008) 4051-4061.
[33] M. Umair, G. Palmisano, R. Al Sakkaf, S.B. Al Jitan, A. Pintar, G. Žerjav, L. Palmisano, V. Loddo, M. Bellardita, Pt-Nb2O5-TiO2 based semiconductors for photo-reforming of glucose and fructose aqueous solutions, Appl. Surf. Sci., (2023) 159030.
[34] L.G. Devi, R. Kavitha, Enhanced photocatalytic activity of sulfur doped TiO2 for the decomposition of phenol: A new insight into the bulk and surface modification, Mater. Chem. Phys., 143 (2014) 1300-1308.
[35] D. Langhammer, J. Kullgren, L. Österlund, Photoinduced Adsorption and Oxidation of SO2 on Anatase TiO2(101), J. Am. Chem. Soc., 142 (2020) 21767-21774.
[36] L. Yang, L.E. Yu, M.B. Ray, Photocatalytic Oxidation of Paracetamol: Dominant Reactants, Intermediates, and Reaction Mechanisms, Environmental Science & Technology, 43 (2009) 460-465.
[37] A. Chatzitakis, C. Berberidou, I. Paspaltsis, G. Kyriakou, T. Sklaviadis, I. Poulios, Photocatalytic degradation and drug activity reduction of Chloramphenicol, Water Res., 42 (2008) 386-394.